Tailoring perpendicular magnetic coupling by XMCD

Y. U. Idzerda, R. Snow, H. Bhatkar, A. T. N'Diaye, and E. A. Arenholz

Citation: AIP Advances **7**, 056306 (2017);
View online: https://doi.org/10.1063/1.4974022
View Table of Contents: http://aip.scitation.org/toc/adv/7/5
Published by the American Institute of Physics

AIP ADVANCES **7**, 056306 (2017)

Tailoring perpendicular magnetic coupling by XMCD

Y. U. Idzerda,[1] R. Snow,[1] H. Bhatkar,[1] A. T. N'Diaye,[2] and E. A. Arenholz[2]
[1]*Department of Physics, Montana State University, Bozeman, Montana 59717, USA*
[2]*Advanced Light Source, Lawrence Berkeley National Laboratory, Berkeley, California 94720, USA*

(Presented 1 November 2016; received 16 September 2016; accepted 25 October 2016; published online 10 January 2017)

The elemental perpendicular magnetic anisotropy constants of both elements of a 20 nm bcc $Co_{88}Mn_{12}$ alloy film grown on MgO(001) and capped with Al, have been determined. By fitting a Stoner-Wohlfarth astroid model to the measured Co and Mn L_3 XMCD peak intensities as a function of incidence photon angle with the magnetic field applied co-axially with the photon propagation direction, the elemental perpendicular anisotropy constants were found to be -6.46×10^5 J/m^3 and -6.68×10^5 J/m^3, respectively. The modeling of the Co and Mn data both result in nearly the same anisotropy constant as expected for a single alloy film. [http://dx.doi.org/10.1063/1.4974022]

I. INTRODUCTION

Quantifying the perpendicular magnetic anisotropy (PMA) of magnetic films and structures has been important in perpendicular magnetic recording media for decades.[1,2] Recently, determining the PMA in thin films systems has gained importance with the discovery and development of magnetic vortex states,[3] magnetic skyrmion systems,[4–6] and in applications of more unique spin-transport electronic structures.[7] For simple systems (magnetic films on non-magnetic substrates) it is straightforward to determine the PMA by a variety of techniques, particularly using ferromagnetic resonance,[8] torque magnetometry,[9] or vector magnetometry.[10–13] This is useful for systems with either a positive (preferring perpendicular moment) or negative (preferring in-plane moment) perpendicular anisotropy constant. Unfortunately, these techniques only measure the total PMA and shed little light on understanding the tailoring of PMA in magnetic heterostructures where separating the contributions to the total PMA in magnetic multilayers or magnetically distinct phases in multi-component systems is needed. In those cases, element-resolved techniques with magnetic contrast would be quite useful.

The use of X-ray magnetic circular dichroism (XMCD) in a vector magnetometry configuration[14] or as the magnetic contrast mechanism in a X-ray microscope[15] has allowed for elemental visualization of PMA, but a quantitative treatment has been lacking. Here we report the determination of elemental PMA constants for a bcc $Co_{88}Mn_{12}$ magnetic alloy film from the variation of the elemental XMCD signal with the applied magnetic field (both magnitude and direction out of the film plane) through a comparison to the Stoner–Wohlfarth astroid modeling of the magnetization.[16–19]

II. EXPERIMENTAL

Tailoring of thin film PMA has been accomplished through composition control of magnetic alloy films and by creating bilayer/multilayer systems with appropriate relative thicknesses. The bcc CoMn alloy film has recently shown[20] to have an increasing saturation moment with composition, reaching a maximum near $Co_{75}Mn_{25}$. Separately determining the PMA constant for the Co and Mn elements in an alloy film would be a good demonstration of the validity of the experimental method.

The bcc $Co_{1-x}Mn_x$ alloy films are grown by molecular beam epitaxy (MBE) on 5 mm x 5 mm MgO(100) substrates. The polished substrates are first rinsed in acetone and methanol, then blown

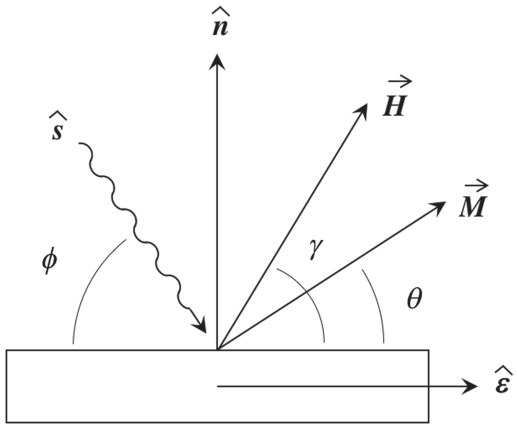

FIG. 1. Experimental configuration showing the magnetization, $\boldsymbol{M}$, of a single domain film with in-plane easy axis, $\boldsymbol{\varepsilon}$, and surface normal, $\boldsymbol{n}$, in an applied field, $\boldsymbol{H}$. The photon propagation direction (analysis direction) is $\boldsymbol{s}$.

dry with dry nitrogen gas prior to mounting on a Molybdenum sample holder using indium solder. Due to the hygroscopic nature of MgO, exposure to water vapor and the typical DI water rinse are avoided. After cleaning and mounting, the samples are heat cleaned in UHV environment at 800°C for 20 minutes to remove adsorbed water and reduce the likelihood of oxidation of the magnetic film.

The elemental Co and Mn flux rates are determined by the stabilized Knudsen cell temperatures of the Co and Mn cells and are approximately 0.1 nm/min and 0.01 nm/min, respectively. For all growths, the substrate was held at 160°C and the sample was capped with 3 nm of Al deposited at 90°C. The bcc film structure was monitored during growth by RHEED, showing bcc epitaxial growth for all films. Details of the growth, including the RHEED pattern evolution, are reported elsewhere.[20,21]

The XAS and XMCD measurements are conducted at beamline 6.3.1.1 and 4.0.2 of the Advanced Light Source of Lawrence Berkeley National Laboratories. Due to the large number of scans, the data is acquired in the fast-scan mode by acquiring sequential energy scans with either opposite magnetizations or opposite photon helicities. Measurements are conducted at room temperature in sample current mode either with the magnetic field co-axial to the photon propagation direction (2T magnet at beamline 6.3.1.1) or with a magnetic field whose direction can be changed (vector magnet at 4.0.2). All spectra are corrected for the degree of circular polarization. This flexibility allows for a wide range of measurement schemes.

As described in Figure 1, through an axial rotation of the sample (ϕ-scan), the angle between the photon propagation direction (analysis direction) and the sample can be varied. In this measurement scheme, the field is held constant and co-axial with the photon propagation direction ($\boldsymbol{H} \parallel \boldsymbol{s}$). In the second measurement scheme (γ-scan), the photon propagation direction is co-axial with the sample normal direction ($\boldsymbol{s} \parallel \boldsymbol{n}$, normal incidence) and the fixed magnitude magnetic field is rotated from being in the film plane to normal to the plane. Finally, the angular orientations can be held constant, but the strength of the magnetic field can be varied (H-scan).

III. RESULTS AND DISCUSSIONS

A description of the characterization of our CoMn alloy films has been described elsewhere.[20] Compositions were determined from XAS intensity ratios and elemental moments from the intensity of the L_3 XMCD features for Co and Mn. The Co and Mn L_{23}-edge XAS and XMCD are displayed in Figure 2 for a 20 nm bcc $Co_{88}Mn_{12}$ film grown on MgO(001) and capped with 3 nm of Al. The data have been corrected for the degree of polarization of the photon and the incident beam direction ($\phi = 30°$ from grazing). The field is applied co-axial with the photon propagation direction ($\gamma = 150°$). Energy calibrations of the Mn and Co edges are accomplished by comparing the measured XAS of

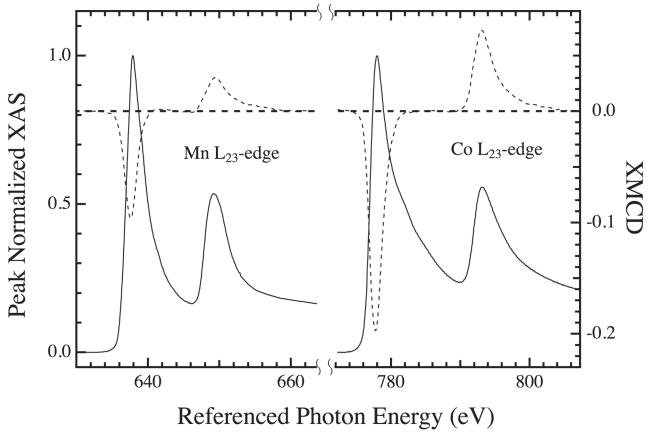

FIG. 2. Co and Mn L_{23} peak XAS (solid lines) and XMCD (dashed lines) for a 20 nm bcc $Co_{88}Mn_{12}$ film grown on MgO(001).

a pure bcc Co film (L_3 peak set to 777.90 eV) or Mn_2O_3 reference powder (L_3 shoulder peak set to 637.97 eV) immediately after the CoMn film and shifting the energy scales.[22]

Figure 3 displays the measured L_3 XMCD dichroism intensity for Co (open squares) and Mn (filled circles) measured as a function of incidence angle for the situation where the magnetic field is applied co-axially with the photon beam propagation direction for a bcc $Co_{88}Mn_{12}$ alloy film. The applied field is ±0.5 T and the angle of incidence (and therefore the applied field direction) is varied by rotating the sample around the z-axis of the XMCD chamber (ϕ-scan). The 0.5 T field intensity is far below the saturation field for the CoMn film. The L_3-peak XMCD intensities are determined by a gaussian-fit to a narrow region encompassing only the L_3-peak.

The data is fit to a Stoner-Wohlfarth (SW) astroid model[16–19] of the projection of the magnetization along the analysis (photon propagation) direction. The SW model was developed for single domain magnetic particles but has been successfully used for thin film systems where the domains

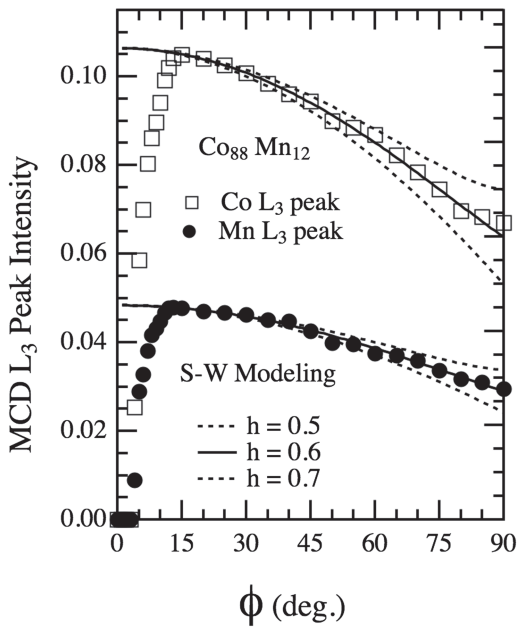

FIG. 3. Co and Mn L_3 peak XMCD as a function of photon incidence angle with the 0.5 T field applied coaxial to the photon incidence direction. Lines are Stoner-Wohlfarth astroid fits for different h values. Both Co and Mn can be modeled using nearly the same elemental PMA value.

can be treated in a mean-filed approach[23] including high density recording media[24] and amorphous films.[25] The fit is controlled by the effective field parameter $h = HM/2K$, with H the applied magnetic field, M the saturation magnetization of the film, and K the perpendicular anisotropy constant. The solid or dashed lines of the two elemental data sets are fits with various h values (the remaining fit parameter is only the vertical scaling) to show the sensitivity of the fit. Possible temperature dependent anisotropy corrections to the SW treatment[26] have not been included.

A least-squares-fit for the Co and Mn data result in an h value of 0.60±0.02 and 0.58±0.02 corresponding to a perpendicular anisotropy constant, K, (at room temperature) of (−6.46±0.15) x 10^5 J/m^3 and (−6.68±0.15) x 10^5 J/m^3, respectively. The increased uncertainty is due to the uncertainty in the determination of M_S. For a bcc CoMn ultrathin film grown on MgO(100) (a_{MgO} = 0.4212 nm), the film is pseudomorphic with the MgO surface, but rotated 45° with respect to the MgO surface net, resulting in a_{CoMn} = 0.2978 nm.[20] Forced registry to a substrate which is not lattice-matched often leads to a tetragonal distortion of the film. Our DFT calculations indicate that the *c/a* ratio at this composition is 0.86 resulting in c_{BCT} = 0.2569 nm. For an average moment of 1.9 μB/atom for $Co_{88}Mn_{12}$, we determine M_S = 1.55 x 10^6 J/m^3-T which results in the above anisotropy constants. Note that the elemental Co and Mn fits both result in nearly the same h value (as expected for a single alloy film and demonstrated here).

If the perpendicular demagnetization factor is known and removed, the remaining anisotropy is due to crystalline anisotropy, surface anisotropy, and interlayer interactions. Repeating these measurements at different temperatures and at different applied field strengths (0.1 T to 0.8 T) can be used to classify these additional anisotropies through their temperature and field dependencies. At low grazing angles (small ϕ), the data diverges from the fit due to overfill issues associated with the grazing x-ray beam spot size and the small sample (and any slight misalignments). These can be easily incorporated into the fit, eliminating the low angle disagreement. The case $\phi = 0$ cannot be measured because the photon is incident parallel to the sample surface. This demonstrates that both elements of a thin film alloy behave identically. The extraction of the perpendicular anisotropy constant is useful, but in this case can be accomplished by other means.

IV. CONCLUSIONS

We have measured the elemental perpendicular magnetic anisotropy for a 20 nm bcc $Co_{88}Mn_{12}$ alloy film grown on MgO(001) and capped with Al. For the bcc $Co_{88}Mn_{12}$ alloy film, the elemental perpendicular anisotropy constants were found to be (−2.92±0.15) x 10^5 J/m^3 and (−3.02±0.15) x 10^5 J/m^3, respectively, from a fit of a Stoner-Wohlfarth astroid model to the measured L_3 XMCD peak intensities for Co and Mn as a function of incidence photon angle.

ACKNOWLEDGMENTS

This material is based upon work supported by the National Science Foundation under Grant ECCS-1542210. The Advanced Light Source is supported by the Director, Office of Science, Office of Basic Energy Sciences, of the U.S. Department of Energy under Contract No. DE-AC02-05CH11231.

[1] M. Oshiki, Journal of Magnetism and Magnetic Materials **324** (3), 351–354 (2012).
[2] J. K. Howard, Journal of Vacuum Science & Technology A **4** (1), 1–13 (1986).
[3] S. K. Kim, M. W. Yoo, J. Lee, H. Y. Lee, J. H. Lee, Y. Gaididei, V. P. Kravchuk, and D. D. Sheka, Scientific Reports **5**, 1 (2015).
[4] V. L. Carvalho-Santos, R. G. Elias, D. Altbir, and J. M. Fonseca, Journal of Magnetism and Magnetic Materials **391**, 179–183 (2015).
[5] W. J. Jiang, P. Upadhyaya, W. Zhang, G. Q. Yu, M. B. Jungfleisch, F. Y. Fradin, J. E. Pearson, Y. Tserkovnyak, K. L. Wang, O. Heinonen, S. G. E. te Velthuis, and A. Hoffmann, Science **349** (6245), 283–286 (2015).
[6] T. Tanigaki, K. Shibata, N. Kanazawa, X. Yu, Y. Onose, H. S. Park, D. Shindo, and Y. Tokura, Nano Letters **15** (8), 5438–5442 (2015).
[7] H. Atsufumi and T. Koki, Journal of Physics D: Applied Physics **47** (19), 193001 (2014).
[8] K. Zakeri, T. Kebe, J. Lindner, and M. Farle, Journal of Magnetism and Magnetic Materials **316** (2), e334–e337 (2007).
[9] C. W. Fleischmann and A. G. Turner, Review of Scientific Instruments **37** (1), 73–77 (1966).
[10] J. A. C. Bland, Journal of Vacuum Science & Technology a-Vacuum Surfaces and Films **15** (3), 1759–1765 (1997).

[11] C. Daboo, J. A. C. Bland, R. J. Hicken, A. J. R. Ives, M. J. Baird, and M. J. Walker, Physical Review B **47** (18), 11852–11859 (1993).
[12] C. Daboo, R. J. Hicken, D. E. P. Eley, M. Gester, S. J. Gray, A. J. R. Ives, and J. A. C. Bland, Journal of Applied Physics **75** (10), 5586–5588 (1994).
[13] C. Morrison, J. J. Miles, T. N. A. Nguyen, Y. Fang, R. K. Dumas, J. Akerman, and T. Thomson, Journal of Applied Physics **117** (17), 4 (2015).
[14] V. Chakarian, Y. U. Idzerda, G. Meigs, E. E. Chaban, J. H. Park, and C. T. Chen, Applied Physics Letters **66** (24), 3368–3370 (1995).
[15] M. Y. Im, K. S. Lee, A. Vogel, J. I. Hong, G. Meier, and P. Fischer, Nature Communications **5**, 6 (2014).
[16] E. C. Stoner and E. P. Wohlfarth, Phil. Trans. Roy. Soc. **A248**, 599 (1948).
[17] I. D. Mayorgoyz, *Mathematical Model of Hysteresis.* (Springer-Verlag, New York, 1991).
[18] L. Vatskitchev, Bulgarian Journal of Physics **26**, 76 (1999).
[19] M. Getzlaff, *Fundamentals of Magnetism.* (Springer-Verlag, New York, 2008).
[20] R. J. Snow, H. Bhatkar, A. T. N'Diaye, E. Arenholz, and Y. U. Idzerda, J. Magn. Magn. Mater. **419**, 490 (2016).
[21] Y. U. Idzerda, H. Bhatkar, and E. Arenholz, Journal of Applied Physics **117** (17) (2015).
[22] C. T. Chen, Y. U. Idzerda, H.-J. Lin, N. V. Smith, G. Meigs, E. Chaban, G. H. Ho, E. Pellegrin, and F. Sette, Phys. Rev. Lett. **75**, 152 (1995).
[23] D. L. Atherton and J. R. Beattie, IEEE Transactions on Magnetics **26**, 3059 (1990).
[24] D. J. Sellmyer, M. Yu, and R. D. Kirby, Nanostructured Materials **12** (5), 1021–1026 (1999).
[25] T. M. L. Alves, C. G. Bezerra, A. D. C. Viegas, S. Nicolodi, M. A. Corrêa, and F. Bohn, Journal of Applied Physics **117** (8), 083901 (2015).
[26] V. Franco and A. Conde, Journal of Magnetism and Magnetic Materials **278** (1–2), 28–38 (2004).